instruments

MDPI

Project Report

Portable Arbitrary Pulse Generator for Driving Microcoils for Micromagnetic Neurostimulation

Robert P. Bloom [1], Renata Saha [1], Zachary Sanger [2], Walter C. Low [3], Theoden I. Netoff [2] and Jian-Ping Wang [1,*]

[1] Department of Electrical and Computer Engineering, University of Minnesota, Minneapolis, MN 55455, USA; bloom261@umn.edu (R.P.B.); saha0072@umn.edu (R.S.)
[2] Department of Biomedical Engineering, University of Minnesota, Minneapolis, MN 55455, USA; sange019@umn.edu (Z.S.); tnetoff@umn.edu (T.I.N.)
[3] Department of Neurosurgery, University of Minnesota, Minneapolis, MN 55455, USA; lowwalt@umn.edu
* Correspondence: author: jpwang@umn.edu

Abstract: Micromagnetic stimulation (μMS) is a promising branch of neurostimulation but without some of the drawbacks of electrical stimulation. Microcoil (μcoil)-based magnetic stimulation uses small micrometer-sized coils that generate a time-varying magnetic field, which, as per Faraday's Laws of Electromagnetic Induction, induces an electric field on a conductive surface. This method of stimulation has the advantage of not requiring electrical contact with the tissue; however, these μcoils are not easy to operate. Large currents are required to generate the required magnetic field. These large currents are too large for standard test equipment to provide, and additional power amplifiers are needed. To aid in the testing and development of micromagnetic stimulation devices, we have created a compact single-unit test setup for driving these devices called the μCoil Driver. This unit is designed to drive small inductive loads up to ±8 V at 5 A and 10 kHz.

Keywords: micromagnetic neurostimulation; microcoils; portable microcoil driver; Faraday's laws of Electromagnetic Induction

Citation: Bloom, R.P.; Saha, R.; Sanger, Z.; Low, W.C.; Netoff, T.I.; Wang, J.-P. Portable Arbitrary Pulse Generator for Driving Microcoils for Micromagnetic Neurostimulation. *Instruments* **2024**, *8*, 55. https://doi.org/10.3390/instruments8040055

Academic Editor: Antonio Ereditato

Received: 2 August 2024
Revised: 30 October 2024
Accepted: 16 November 2024
Published: 16 December 2024

1. Introduction

In the field of neurostimulation, micromagnetic stimulation (μMS) is a promising alternative to electrical stimulation. Possible applications include the treatment of Parkinson's, epilepsy, dystonia, tremors, and OCD [1–7]. Both methods stimulate neurons by generating an electric field; however, they differ in how the electric field is created. Electrical stimulation generates electric field by applying a voltage across implanted electrodes, whereas μMS uses a time-varying magnetic field to induce an electric field in the neuron. Although electrical stimulation has provided desirable results, those electrical electrodes require galvanic contact with tissues, leading to biofouling and encapsulation of the electrode [1]. Micromagnetic stimulation is an alternative that overcomes this drawback associated with electrodes, as they do not require galvanic contact with the tissue.

The devices used in μMS are popularly known as microcoils (μcoils). They are small coils of wire that generate a directed magnetic field when current flows through them. Custom coils can be fabricated as in Refs. [8–10], or commercially available inductors as Refs. [11–13] used in circuit designs can be used [1]. In general, these coils tend to show very low impedances. This characteristic, along with the large currents required to produce suitable magnetic fields from the μcoil, make them difficult to drive. Standard test equipment cannot provide the required power, and a power amplifier is required. A typical electrical setup for micromagnetic stimulation consists of a waveform source (function generator or digital-to-analog converter), a power amplifier, and occasionally a PC [11,13–15]. Multi-unit test setups make transport more difficult during transition to clinical settings as they require more lab space.

Our goal was to condense the typical test setup into a single compact unit. A unified system allows for ease of testing and portability, is well suited for testing across multiple labs, and enhances the ease of transitioning the technology into clinical settings. In addition, the unit is battery-powered to help mitigate any interference or noise from the power lines. This is of huge advantage while recording electrophysiological signals from the brain, as the recorded signals will not be affected much by the power line noise, thereby facilitating ease of data analysis. In this work, we present a portable, battery-powered, 40 W arbitrary pulse generator designed specifically to work with the Magnetic Pen (MagPen) [11] set of devices, as well as other micrometer-sized inductors. In our previous work [11], the MagPen system was developed and tested on rat hippocampal slices, and a strength–frequency curve was generated. From this work, the minimum operating parameters for the MagPen µcoil were found to be 500 mA at 2 kHz. The MagPen system has also been characterized for stimulating the sciatic nerve of a rat [16], in which successful stimulations were recorded with stimulation frequencies from 500 Hz to 5 kHz with coil current as low as 50 mA. The prototyped unit reported in this work, better named the µcoil Driver, provides the basic functionality required by the typical MagPen µcoil experiment. Future work may include expanding the functionality of the unit, such as increasing the output power and output frequency range, as well as adding additional output channels and synchronization to external inputs. This will allow the unit to better accommodate various coil and experimental requirements.

A similar driving circuit was described in [17]. Their unit was designed to drive similar coils using higher-frequency continuous sin waves. The primary difference is the types of waveforms generated; the µcoil Driver is designed to generate arbitrary waveform pulses at lower frequencies.

The rest of this article is organized as follows: The design specifications, circuit design, MagPen fabrication, and experimental setup are detailed in Section 2. Section 3 covers the device operation and the results of animal testing. Discussion and conclusion of the results are presented in Sections 4 and 5, respectively.

2. Methods and Procedures

The MagPen system, as reported by Saha et al. [11], is a micrometer-sized coil (µcoil) used to stimulate neurons. Current is driven through the coils to generate a localized magnetic field, which in turn generates an electric field in the neurons. These coils operate in two regimes: low-frequency activation and high-frequency suppression. In the low-frequency regime, typical operation consists of driving a 1–2 A sinusoidal pulse at frequencies of 1–5 kHz. At these frequencies, the µcoils behave as a resistor with parasitic inductance. Therefore, there is no appreciable phase shift and they can be treated as a low-resistance load. In most experiments, the µcoils are driven up to 5 A (rarely 10 A, as reported in [12]) to evoke a response [11].

2.1. Physical Structure of the µCoil Driver

The µCoil Driver's physical design was influenced by the goals of small form factor and desired battery life. The overall size of the unit was largely determined by the chosen batteries, with extra space allotted for the circuitry and wiring (Figure 1d). The front of the unit, shown in Figure 1a, features a touch-screen display, status LED, output and USB ports, and the power button. For ease of use, the user is given a touch interface and menu-style navigation, where user inputs and operations are reinforced by a status LED and audible beeps. The status LED displays whether the output is ON or OFF, as well as any system errors. Error messages are conveyed by the color and blinking of the status LED, beeping, and error messages on the screen. A custom cable connects the output port to the µcoil. The USB port allows for arbitrary waveforms to be loaded from a PC. The back of the unit (Figure 2b) contains battery fuses, the battery charging port, an external power port, and the power selector switch. The power selector switch allows for the unit to operate using its internal batteries or from an external power source. The unit measures 152 mm wide,

255 mm long, and 110 mm tall and weighs 4.7 kg. This compact form factor allows for the µCoil Driver to be easily transported between labs and to require minimal lab space. The unit is also small enough to fit in medium-shielded test setups.

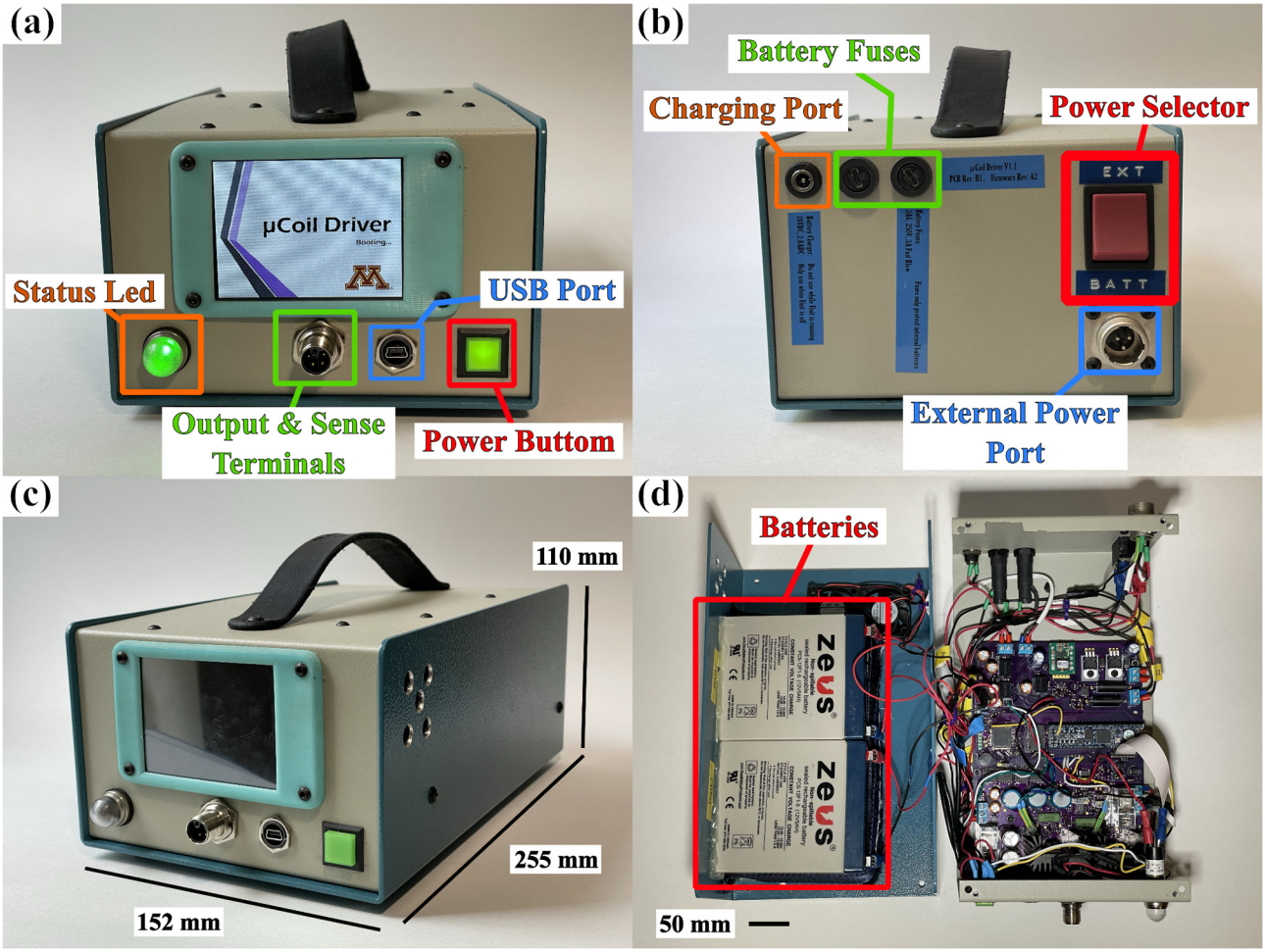

Figure 1. (**a**) µCoil Driver front panel. (**b**) µCoil Driver back panel. (**c**) µCoil Driver unit. (**d**) µCoil Driver internals.

2.2. µCoil Driver: Circuit Overview

The µCoil Driver circuit can be broken into 3 main pieces (see Figure 2b): battery charger, digital, and analog sections. The battery charger is a stand-alone circuit on the same PCB and is only active when the unit is in charging mode. The circuit charges the two 12 V batteries independently using a two-stage charging scheme. The charger is an analog circuit with a PIC12 microcontroller providing charge indication to the user and monitoring for even charging.

The digital section (see Figure 2) of the µCoil Driver is responsible for running the graphical user interface (GUI), waveform calculation, and system monitoring. These tasks are divided amongst three programmable devices: 4D Systems smart display, Xilinx Artix 7 FPGA, and PSOC5 microcontroller. The 4D Systems display module is a touch-screen LCD with integrated microprocessor. The interface was programmed using 4D Systems' standard widgets and development software. It is responsible for running the GUI and passing information between the user and the PSOC5 microcontroller. The GUI allows for the user to select the output waveform and turn ON and OFF the output. The GUI also passes system information back to the user, like battery charge and error messages.

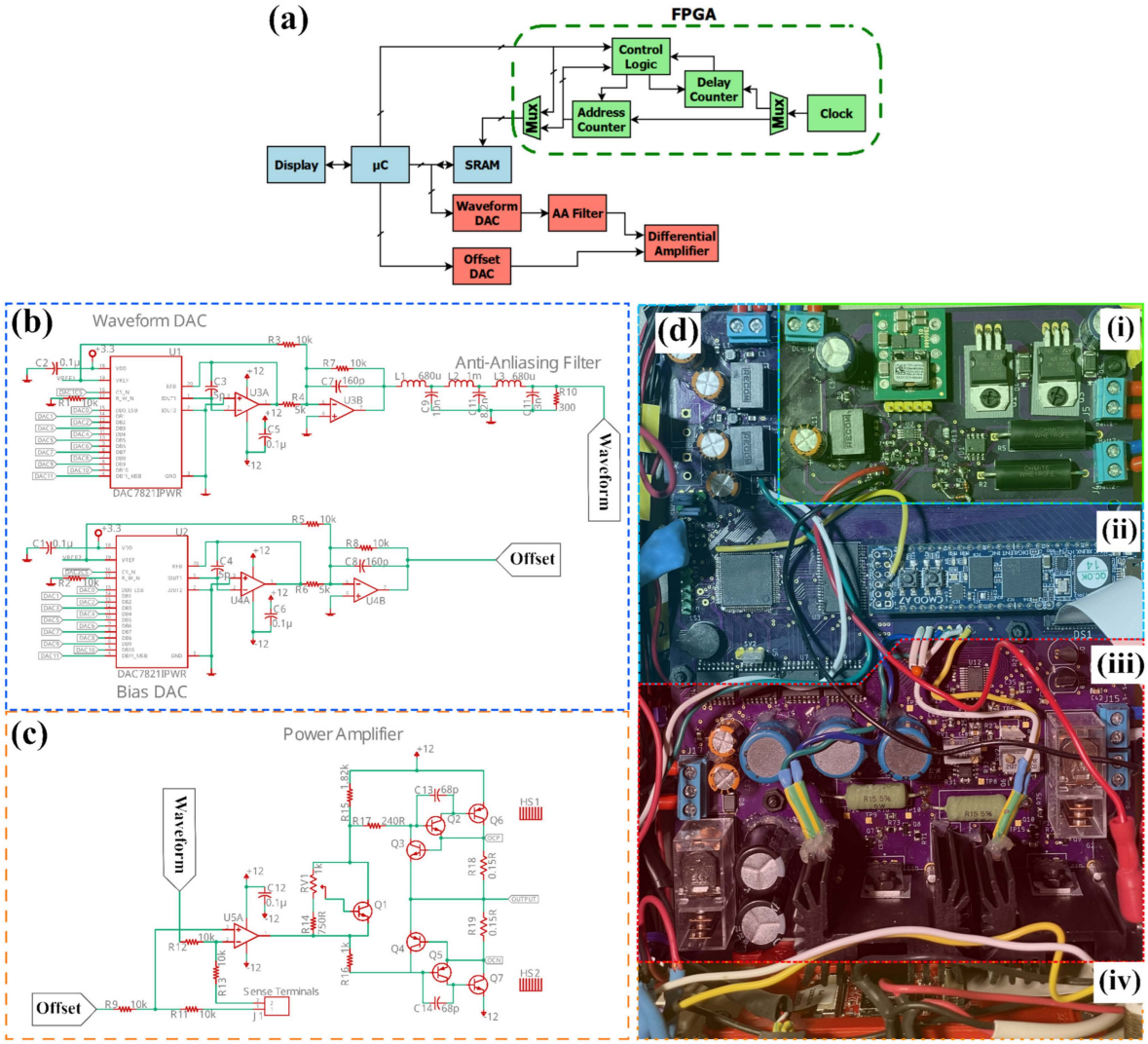

Figure 2. (**a**) µCoil Driver functional diagram. (**b**) Waveform generation section. (**c**) Power amplifier section. (**d**) PCB sections: (**i**) battery charger, (**ii**) digital section, (**iii**) analog section, and (**iv**) display.

The user-selected waveform is passed from the display to the microcontroller, which then calculates and loads the waveform into a static random-access memory (SRAM) IC. In remote load mode, the waveform is calculated by the PC and loaded onto the SRAM, where the microcontroller acts as an intermediary. The PSOC5 microcontroller is also responsible for monitoring the system. This includes managing the USB and UART communication interfaces, temperature and fan control, battery monitoring, managing various ICs, and output over current. To manage the large number of tasks and to allow for easy expansion, the PSOC5 microcontroller is running the FreeRTOS real-time operating system [18]. The operating system runs with 1 ms ticks, and therefore, precise timings and synchronizing the output are not possible.

Once the waveform is loaded into the SRAM, the next step is to pass the data to the digital-to-analog converters (DACs). This action is completed by the FPGA, whose primary role is as a direct memory access controller (DMA). An FPGA was used for this to ensure consistent timing. It also allows for future expansion to include synchronizing the output to an input trigger and to synchronize multiple units for driving arrays of coils. Once the data has been transferred from the SRAM to the DACs, the output waveform enters the analog section of the circuit.

The analog section of the circuit starts with the DAC and ends with the power amplifier. The signal path begins with a pair of DACs. One DAC is connected to the SRAM and is

used for waveform generation. The second DAC generates a DC bias and is primarily used to remove any offsets that exist along the signal path. The output of the waveform DAC is passed through an anti-aliasing filter to remove the high-frequency components of the quantized signal. The waveform and bias signals are combined using a differential amplifier. The differential amplifier was designed with a gain of 1 v/v and regulates the output voltage at the load using sense terminals. The differential amplifier consists of an operation amplifier (op amp) and a class AB power amplifier stage to increase the maximum output current. To help minimize any noise generated by the digital section, the analog and digital circuits have separate grounds and are connected via digital isolator ICs.

2.3. µCoil Driver: Circuit Design

The specifications of the output state were determined largely by our previous work in which we characterized the MagPen system on rat hippocampal slices as well as the rat sciatic nerve [11,16]. From both of these works, the required coil current decreases with increasing frequency; however, the required current begins to flatten at frequencies above 2 kHz. In both experiments, the stimulus frequency ranged from 100 Hz to 5 kHz and coil currents from 25 mA to 5 A [11,16]. Other works on µcoil-based stimulation noted stimulation frequencies of 1 Hz–3 kHz, with some using a frequency of 70 kHz [1,10,12–14,19–22]. Neurons' electrical nature is like a low-pass filter [23–25]. The membrane dynamics of the neurons act to filter out frequencies above 5 kHz. The typical current draw for stimulation was around 1 A–3 A, with the maximum current requirements in the order of 5 amps, depending on coil and stimulation frequency [1,10–12,17]. The MagPen system's µcoils have an inductance of 600 nH and a series resistance of 2 Ω. Other works report µcoil inductances ranging from ~40 nH to ~1 µH and series resistances ranging from ~1 Ω to ~7 Ω [1,10–12,16,17,26]. A commonality between the various coils is that at low frequencies used for stimulation, the coils can be treated as resistors with a parasitic inductance. Using the MagPen system's µcoils as a baseline, the waveform voltage needs to span ±10 V to drive the µcoils with a current of ±5 A. To accommodate the majority of coils and stimulation waveforms, the goal was to design a driver capable of generating arbitrary waveforms up to ±10 V at frequencies up to 10 kHz while providing current up to ±5 A. To better meet the requirements of other coils and experiments, the design of the driver should be flexible such that the output parameters can be modified by swapping out a minimal number of circuit components.

Waveform generation is achieved by storing the waveform datapoints in an SRAM and streaming the data into a DAC to produce the voltage waveform. The DAC's sampling rate needs to be no slower than the Nyquist rate for fastest waveform, which is 20 kHz in this design. Using a sampling rate of 20 kHz would complicate the design of the antialiasing filter. The concern is that in practice, a filter for a sampling rate of 20 kHz would likely cause noticeable distortion at 10 kHz. To better guarantee signal fidelity and to lessen the requirements of the antialiasing filter, a faster sampling rate of 200 kHz was chosen for the final design. This frequency is 10× higher than the Nyquist rate for 10 kHz and gives more margin of error for the subsequent circuits along the signal path. An additional benefit is that the system is more readily able to be upgraded to higher output frequencies.

The DACs chosen for this design are the DAC7821. This series of DACs has a 12-bit resolution and an external voltage reference. Three reference voltages of 2.048 V, 4.096 V, and 8.192 V are available to the DAC and are selected via an analog multiplexer. This was done to ensure that smaller waveforms could be generated at a high resolution to better accommodate low impedance coils. The DAC7821 series DAC is designed to generate a unipolar voltage output when paired with a current-to-voltage amplifier (U3A and U4A in Figure 2b). To produce the bipolar signal, the output of the DAC is passed through an amplifier that doubles and offsets the signal such that the midpoint of the range is at 0 V (U3B and U4B in Figure 2b). This results in the middle DAC code, 0b100000000000, corresponding to 0 V, and an output swing of plus-minus the reference voltage. For the waveform DAC, there is an additional circuit following the amplifier, an anti-aliasing filter

(AA filter). The purpose of the AA filter is to smooth out the stepped waveform generated by the DAC. To minimize the distortion of signals up to 10 kHz, the filter's cutoff frequency was chosen to be 50 kHz. The 50 kHz cutoff frequency also allows for waveforms with higher frequency components (e.g., square waves) to be generated with an acceptable amount of peaking and ringing. A 3rd order Chebyshev filter was used to ensure a clean waveform. This filter also sets the upper frequency limit of the μCoil Driver. Higher output frequencies can be easily attained by changing the cutoff frequency of the AA filter and increasing the sampling rate.

The final stage of the signal path is the power amplifier. This stage consists of a differential amplifier, power output stage, and sense terminals. The inputs of the differential amplifier are conditioned waveforms generated by the two DACs. Feedback to the amplifier is provided by the sense terminals. The sense terminals provide a low current path to sense the voltage at the load; this is done to mitigate the voltage drop over the output cabling. To provide the high current required to drive the coils, a power amplifier was placed between the differential amplifier and the sense terminals. A class AB output stage was chosen for its low distortion, push–pull output, and lower power consumption (compared to a class A output stage). In this design, the main drive transistors consist of a Sziklai pair. The Sziklai pair provides the higher gain required to generate the large currents from the lower voltages available in a battery-power design. In addition, the Sziklai pair allows for a higher output swing compared to a Darlington pair. This is due to the output swing being limited by the Vbe voltage of the transistor pair. The output stage is biased using a Vbe multiplier. Feedback stability is provided by a Miller capacitor placed across the first transistor in the Sziklai pair.

To power the μCoil Driver, batteries were desired to allow for the unit to be isolated from the other test equipment and earth. This specification limited the available supply voltages. A pair of 12 V lead acid batteries (Zeus PC5-12F1) were chosen for their ease of use, availability, and voltage. Running on fully charged batteries, the μCoil Driver can generate an output swing of ±10 V. However, the output swing drops as the batteries discharge. When the batteries are nearly fully discharged, the max output swing is reduced to only ±8 V. In order to have a reliable output and a constant output swing over the entire charge cycle, the amplitude of possible waveforms was software limited to ±8 V.

The resulting design is capable of generating voltage waveforms of ±8 V while supplying up to ±5 A. Waveforms of up to 10 kHz can be accurately generated, with the corner frequency of the driver being 50 kHz. All of the desired specifications were met except for the output swing, which is 2 V lower than goal of ±10 V.

2.4. Fabrication of the MagPen Prototype

The MagPen prototype was prepared for the demonstration of the μCoil Driver in the same way as reported in Ref [11]. Inductors that were commercially available were soldered using solder flux and hot air blower on to the tip of a printed circuit board (PCB). The PCB thickness was thinned down to 0.4 mm into a semi-rigid structure to facilitate an easy adjustment of the MagPen prototype over the nerve. Of the two kinds of MagPen prototypes reported in our earlier work [11], MagPen: Type V successfully activated the sciatic nerve. Just as reported earlier, a 10 μm thick Parylene-C coating was provided at the tip of the μcoil just to ensure the cause for sciatic nerve activation was not from the leakage current.

2.5. Animal Surgery and Experimental Set-Up

Surgical methods and anesthesia regimens were conducted under a University of Minnesota Institutional Animal Care and Use Committee (IACUC)-approved protocol 2004-38001A, similar to our work reported in [16]. Device testing was conducted in vivo in two Long–Evans (L/E) rats weighting 354.5 ± 94.05 g. Urethane (1200 mg/kg) was delivered through intraperitoneal injection, and proper sedation was assessed through toe pinch prior to local anesthesia and subcutaneous delivery of 4 mg/kg Lidocaine and

2 mg/kg Bupivacaine at the site of incision. Urethane anesthesia was chosen over other approaches to preserve neurotransmitter release mechanisms. Heating devices were placed under the animal to maintain homeostasis while supplemental oxygen was administered via nose cone. A 30 mm incision perpendicular to the nerve exposed the dorsal–medial right quadricep muscular interstitial space. One cotton-tipped applicator elevated the sciatic nerve from the interstitial space to space the nerve away from the muscle for effective placement of the µcoil. Throughout the surgery and micromagnetic coil stimulation, anesthetic depth and vital signs were checked every 15 min to ensure animal comfort and homeostasis.

3. Results

3.1. µcoil Driver: Operation

The µCoil Driver is powered by two 12 V batteries and can achieve a maximum output swing of ±8 V with a maximum peak current of 5 A. Under standard test settings of 1 kHz and 3 A pulses occurring every second, the unit is expected to have a battery life of 5 hrs. Alternatively, the unit can be easily switched to an external power source for longer-duration tests.

The onboard GUI allows the user to select sinusoidal pulses. The pulse parameters are frequency, amplitude, phase, cycle count, and interval (see Figure 3a,b). Frequencies can be selected up to 50 kHz with a step size of 1 Hz. The amplitude (Vpeak) is selectable from 0 V to 8 V in 1 mV steps. Phase can be chosen from 0° to 359° in 1° increments. Generated pulses idle at the last point. When the waveform is calculated, it will automatically offset the sinusoid such that it starts and stops at 0 V. For example, a sinusoidal pulse with a phase shift of 90° will generate a single-sided negative pulse. The cycle count is the number of periods of the sinusoid per pulse and can be selected from 1 to 99 cycles (see Figure 3c). Lastly, the interval is the delay between the pulses. This can be selected from up to 10 sec at a resolution of 1 ms. Another feature is the ability to set the number of bursts. The user can select 1–5 bursts; each burst is customizable with the parameters above. When using multiple bursts (see Figure 3d), each burst will be generated consecutively, with the desired interval between bursts before repeating.

Alternatively, arbitrary waveforms can be generated on a PC (see Figure 3e–g) and passed to the unit via USB. The unit identifies the PC as a COM (communication) port. MATLAB was used to generate the waveforms and load them onto the unit. The 8 Mb SRAM accommodates waveforms of up to 2.5 sec in duration. Arbitrary waveforms must conform to the same limitations as the sinusoidal waveforms described above. Multiple bursts are also supported in this mode. The PC interface allows for basic control of the device, such as turning the output ON and OFF.

The performance of the unit was validated by measuring the output waveforms for frequency and amplitude accuracy with and without a load. The DC offset of the output was measured at 115 µV using a Rigol DM3058E multimeter. To measure the accuracy of the output frequency, the driver was set to output a continuous waveform, which was measured using a Rigol DG1022 frequency counter. The output frequency was accurate to ±0.01% across the range of operations. A Rigol DS1051 oscilloscope was used to measure the voltages, showing the output amplitude to be accurate to ±3%. Sinusoidal outputs were also measured by a Rigol DM3058E to an accuracy of ±1%. The error measurements are within the stated measurement error of the test equipment. Therefore, it is likely that the output voltage accuracy is higher than that measured with a theoretical max error of 0.3% due to the resolution of the DAC.

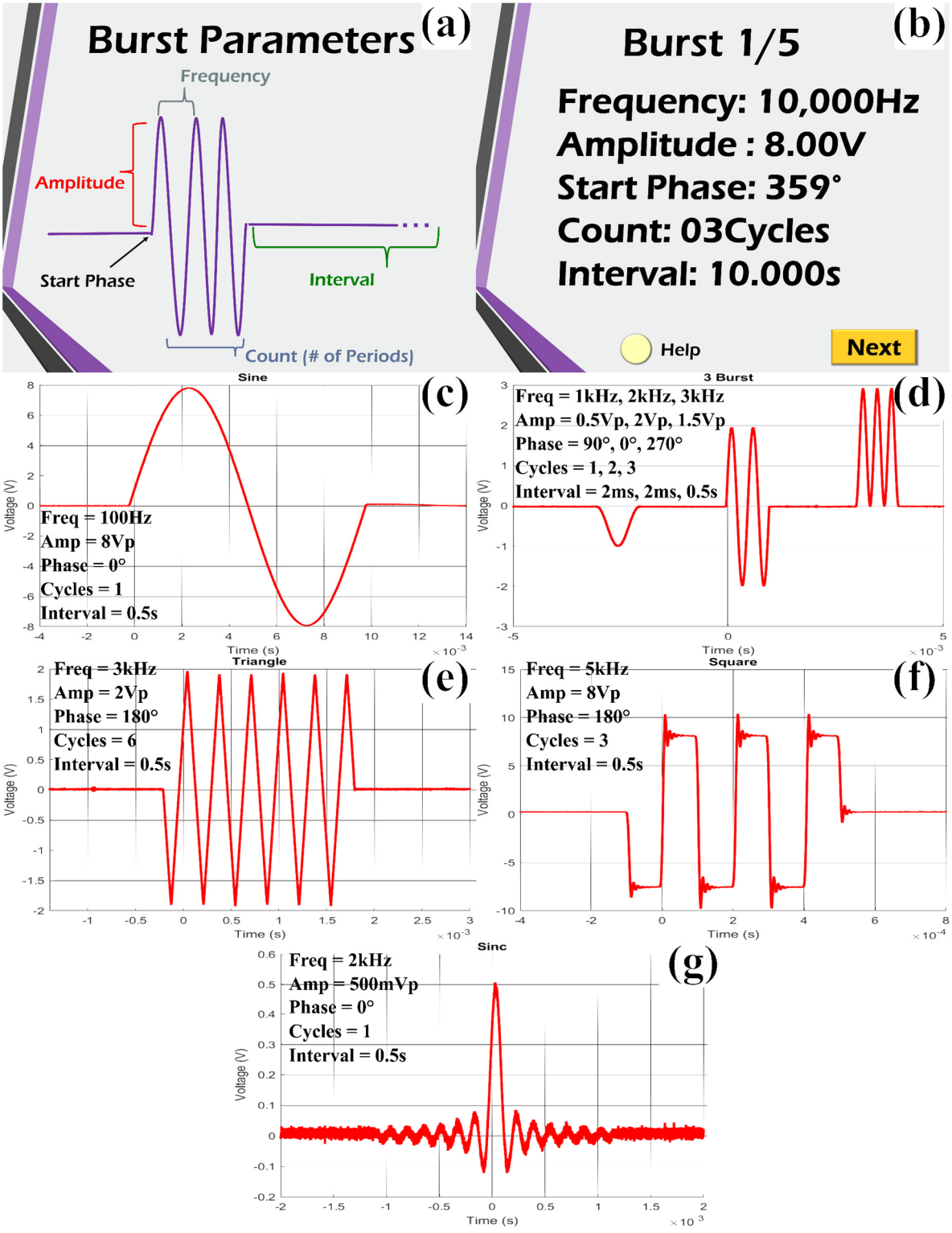

Figure 3. (**a**) Waveform parameter definitions (help menu). (**b**) Waveform selection menu. (**c**) Sinusoidal output. (**d**) Three burst outputs. (**e**–**g**) arbitrary waveform outputs: triangle, square, and sin, respectively.

The output voltage of the driver is regulated and will not vary with load. The output current can be determined using the coils' impedance and Ohm's Law. The MagPen system's µCoil can be well represented by the standard parasitic model for an inductor, shown in Figure 4a. For sinusoidal waveforms, the impedance of a µcoil can be calculated

using Equation (1). The coil current can then be calculated using Ohm's Law, shown in Equation (2). For the MagPen system and other similar coils, the parallel capacitor (C_p) is very small and can be ignored. Figure 4b–d shows the output voltage and resulting current waveforms for various coils. The MagPen µcoil is shown in Figure 4b, and a similarly sized coil in Figure 4c. These coils display a negligible phase shift; their behavior is dominated by their parasitic resistance (R_p). A larger inductor is shown in Figure 4d to show the possible phase shift.

$$Z_{coil} = (j\omega L + R_p) \parallel \frac{1}{j\omega C_p} \tag{1}$$

$$I = V / Z_{coil} \tag{2}$$

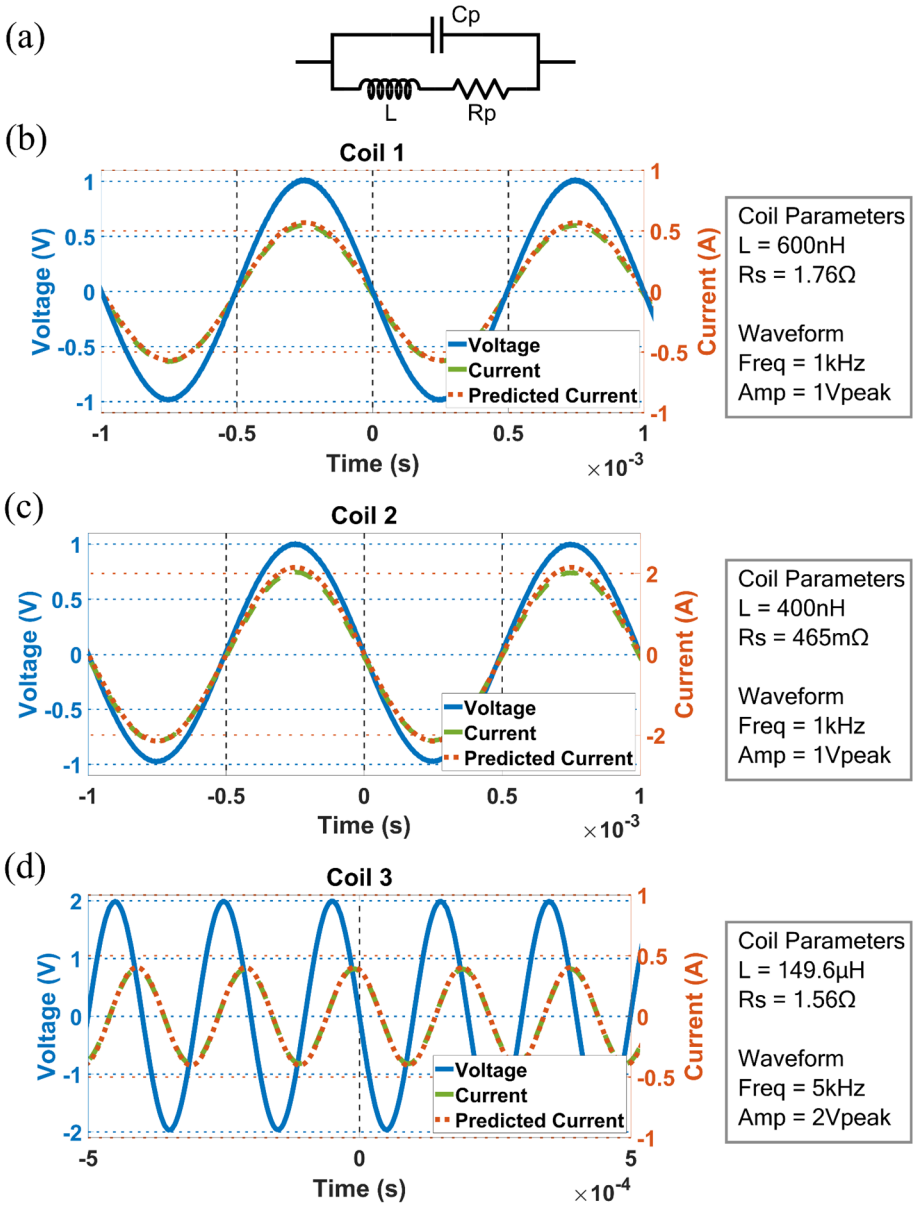

Figure 4. (**a**) Circuit model of inductor parasitics, which can be used to calculate output current waveform. (**b**–**d**) Plots of measured output voltage and current as well as the predicted current waveforms for various inductive loads. (**b**,**c**) show a couple of µcoils with values typical to those used in micromagnetic stimulation. These coils show a primarily resistive behavior. (**d**) shows a larger inductive load whose impedance is largely due to the coils inductance, resulting in a notable phase shift.

3.2. µcoil Driver: Animal Testing

The testing consisted of validating the functionality of the unit and comparing it to the test setup used by [11] for the MagPen system. The unit was validated by driving the MagPen devices to stimulate the sciatic nerve of a rat. Magnetic field pulses applied to the sciatic nerve can invoke a response from the rat in the form of a sudden leg movement. Control tests were first performed using bipolar electrodes (Plastics One Model No. MS303/8C) used for electrical stimulation as well as the original MagPen driving system [11]. This gave a reference for the physical position of the MagPen device as well as the driving waveform parameters needed to invoke a response. Performing these control tests was essential, as there are several reports in the past portraying orientation-dependent activation of neurons from these µcoils [11,12,15].

The complete experimental setup with the portable µCoil Driver powering the MagPen system held over the rat sciatic nerve has been shown in Figure 5a. Testing consisted of applying voltage pulses of varying wave shape and amplitude and looking for a response from the animal. The MagPen under test had a resistance of 1.8–2 Ω and an inductance of 0.6 µH. Pulse voltages were chosen to operate the MagPen system over a range of currents across its typical operating range. Biphasic and monophasic waveforms were tested for the following waveforms: sinusoidal, square, and triangular (see Table 1). Upon successful stimulation of the sciatic nerve, we see the limb muscle of the rat hind limb twitching. By 'Pass' (marked in GREEN), we mean a successful observation of the leg muscle movement. By 'Fail' (marked in RED), we mean that leg muscle movement was not observed upon MagPen stimulation when powered by the portable µCoil Driver. Waveform parameters were set for a frequency of 1 kHz, a count of 1 cycle, and an interval of 1 sec. The amplitude of the signal was varied, showing the sensitivity of the animal's response. The tests were also repeated for phases of 0°, 90°, and 270°. A phase of 0° represents a biphasic pulse, whereas 90° and 270° are monophasic. The results of testing are shown in Table 1.

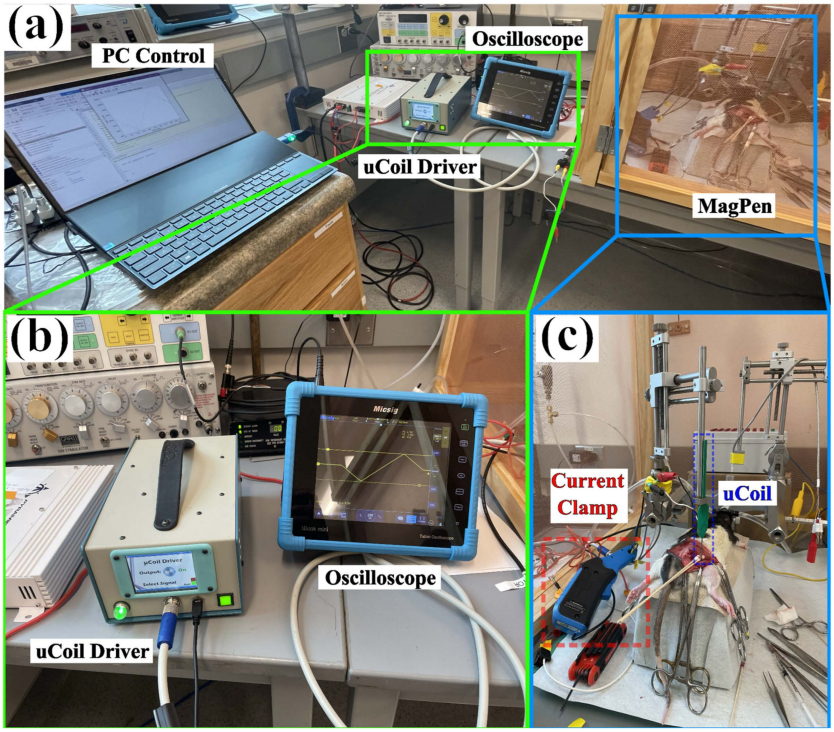

Figure 5. (**a**) Experimental test setup consisting of PC, µCoil Driver, oscilloscope, and MagPen (**b**) µCoil Driver output on, with oscilloscope monitoring the output current. (**c**) Surgery setup with MagPen µcoil placed over rat sciatic nerve.

Table 1. Results of μCoil Driver and MagPen stimulation of rat sciatic nerve.

MagPen Sciatic Nerve Stimulation				
Frequency		**Interval**		**Cycles**
1 kHz		1 sec		1 cycle
Sin		**phase**		
		0°	90°	270°
amplitude	$5V_{pp}$	pass	fail	pass
	$4V_{pp}$	pass	fail	pass
	$2V_{pp}$	pass	fail	pass
	$1V_{pp}$	fail	fail	fail
Triangle		**phase**		
		0°	90°	270°
amplitude	$5V_{pp}$	pass	fail	pass
	$4V_{pp}$	pass	fail	pass
	$2V_{pp}$	pass	fail	fail
	$1V_{pp}$	fail	fail	fail
Square		**phase**		
		0°	90°	270°
amplitude	$5V_{pp}$	pass	pass	pass
	$4V_{pp}$	pass	pass	pass
	$2V_{pp}$	pass	fail	pass
	$1V_{pp}$	fail	fail	fail

From Table 1, we see that the MagPen stimulation of the sciatic nerve failed to evoke a leg muscle twitch for all waveform shapes and all phases of the 1 Vp-p amplitude driving the μcoil. This can be explained as follows: First, 1 Vp-p amplitude when driving a μcoil of resistance of about 2 Ω means that only 0.5 A of current is powering the μcoil. This current is too low to activate the nerves. In contrast, when 2 Vp-p, 4 Vp-p, and 5 Vp-p are driving the μcoil, we observe that the leg muscle twitches at 0° and 270° but not at 90°. This is because at 0° and 270°, the waveforms start at 0 Vp-p and reach the positive maximum Vp-p at 1/4th of the total duration (here, total duration = 1/1 kHz = 1 msec; so, 1/4th of the total duration = 250 μsec); then reach 0 Vp-p at ½ of the total duration (here, 500 μsec). Then again, they reach the negative maximum Vp-p at 3/4th of the total duration (here, 750 μsec) until they finally reach 0 Vp-p at 1 msec again. So, the nerve is expected to activate throughout the positive maximum and negative maximum during the durations of 500 μsec each. But, in the case of the 90° phase (for sines and triangles), the waveform starts at a positive maximum and then drops to 0 Vp-p at 250 μsec. In this short duration, the nerve cannot get activated; hence, we do not see any leg muscle movement. For the square waves, we still observe leg muscle movement at higher amplitudes—4 Vp-p and 5 Vp-p at 90° phase—because the square wave remains at the maximum positive and negative amplitudes throughout the 250 μsec durations and does not attenuate rapidly as for sine and triangular waves.

4. Discussion

Functionally, the μCoil Driver provides a more limited set of electrical outputs when compared to the original test setup. Its advantages are that it is a single unit, is battery powered, and has a small form factor. The onboard batteries are large enough to power the unit for up to five hours of continuous testing. For longer tests, the unit can be switched to an external power source. An additional advantage of being battery operated is that

the unit can be isolated from noisy and intermittent wall power. The small size of the unit offers portability and can be used in small to medium shielded enclosures.

Another advantage comes from the power amplifier. The μCoil Driver uses a class AB amplifier, whereas the original MagPen driving system utilized a class D amplifier [11]. The μCoil Driver can produce cleaner signals without the characteristic high-frequency noise of class D amplifiers. This design decision favored higher signal fidelity at the cost of lower driving power and shorter battery life.

Though the electrical characteristics of the μCoil Driver offer little benefit over the current setup, the μCoil Driver provides a basic platform that can be expanded upon. Future work may include higher output power, more channels, or synchronization between multiple units.

5. Conclusions

In this work, we have presented the μCoil Driver—a portable, battery-powered, 40 W arbitrary pulse generator—designed specifically to work with the micromagnetic neurostimulators and facilitate the ease of carrying the driving unit across different experimental and clinical settings. The μCoil Driver can produce output waveforms (sine, square, triangular, arbitrary) with an upper limit of the voltage in the orders of ± 8 V and a current and frequency rating of 5 A and 10 kHz, respectively. The unit is compact and easy to transport between labs. In vivo experiments on rat sciatic nerve stimulation further validated and experimentally demonstrated that the μCoil Driver can effectively drive the MagPen system as efficiently as the standard test setup. This unit provides the basic functionality needed for micromagnetic stimulation operations and can serve as a basic building block on which other features can be added.

Supplementary Materials: The following supporting information can be downloaded at https://drive.google.com/drive/folders/1RxELYqTsQiPRGta50EE1b2IrqBlxuCHv?usp=sharing (accessed on 1 August 2024): Videos of experiments using various stimulation pulses are provided in the Supplementary Material. All the experiments shown follow the setup described in Section 3.2 and shown in Figure 5. Each video records a different stimulation pulse. The videos show the chosen stimulation voltage pulse on the computer (as DAC codes), the measured output current waveform on the oscilloscope, and the animal's response. The parameters of the stimulation pulse used in each video are listed below. **SV1:** Sine wave, 1 cycle, 1 kHz, 10 Vpp; **SV2:** Half sine wave, 1 cycle, 1 kHz, 5 Vpp; **SV3:** Square wave, 1 cycle, 1 kHz, 10 Vpp; **SV4:** Half square wave, 1 cycle, 1 kHz, 5 Vpp; **SV5:** Triangle wave, 1 cycle, 1 kHz, 10 Vpp; **SV6:** Half triangle wave, 1 cycle, 1 kHz, 5 Vpp; **SV7:** Arbitrary pulse, 1 cycle, 2 kHz, 12 Vpp.

Author Contributions: Conceptualization, All authors; Methodology, R.P.B. and R.S.; Software, R.P.B.; Validation, R.P.B., R.S. and Z.S.; Formal Analysis, R.P.B. and R.S.; Investigation, R.P.B., R.S. and Z.S.; Resources, T.I.N. and J.-P.W.; Data Curation, R.P.B., R.S. and Z.S.; Writing—Original Draft Preparation, R.P.B. and R.S.; Writing—Review & Editing, All authors; Visualization, R.P.B.; Supervision, W.C.L., T.I.N. and J.-P.W.; Project Administration, J.-P.W.; Funding Acquisition, J.-P.W. All authors have read and agreed to the published version of the manuscript.

Funding: This study was financially supported by the Minnesota Partnership for Biotechnology and Medical Genomics under award number ML2020. Chap 64. Art I, Sec11on 4. R.S. acknowledges the 3-year College of Science and Engineering (CSE) Fellowship awarded by the University of Minnesota, Twin Cities. Research reported in this publication was supported by the University of Minnesota's MnDRIVE (Minnesota's Discovery, Research and Innovation Economy) initiative. Portions of this work were conducted in the Minnesota Nano Center (MNC), which is supported by the National Science Foundation through the National Nano Coordinated Infrastructure Network (NNCI) under Award Number ECCS-2025124.

Data Availability Statement: All collected data is presented in the article and Supplementary Material.

Acknowledgments: The authors would also like to thank useful discussions with Winfried A. Raabe, from the Department of Neurology; Kendall H. Lee; Charles D. Blaha; and Yoonbae Oh, from Mayo Clinic, Rochester, MN. J.P.W., R.P.B. and R.S. also thank the Robert Hartmann Endowed Chair support.

Conflicts of Interest: The authors declare no conflicts of interest.

References

1. Saha, R.; Wu, K.; Bloom, R.P.; Liang, S.; Tonini, D.; Wang, J.P. A review on magnetic and spintronic neurostimulation: Challenges and prospects. *Nanotechnology* **2022**, *33*, 182004. [CrossRef] [PubMed]
2. Bouthour, W.; Mégevand, P.; Donoghue, J.; Lüscher, C.; Birbaumer, N.; Krack, P. Biomarkers for closed-loop deep brain stimulation in Parkinson disease and beyond. *Nat. Rev. Neurol.* **2019**, *15*, 343–352. [CrossRef] [PubMed]
3. Habets, J.G.; Heijmans, M.; Kuijf, M.L.; Janssen, M.L.; Temel, Y.; Kubben, P.L. An update on adaptive deep brain stimulation in Parkinson's disease. *Mov. Disord.* **2018**, *33*, 1834–1843. [CrossRef] [PubMed]
4. Dell, K.L.; Cook, M.J.; Maturana, M.I. Deep Brain Stimulation for Epilepsy: Biomarkers for Optimization. *Curr. Treat. Options Neurol.* **2019**, *21*, 47. [CrossRef]
5. Rodrigues, F.B.; Duarte, G.S.; Prescott, D.; Ferreira, J.; Costa, J. Deep brain stimulation for dystonia. *Cochrane Database Syst. Rev.* **2019**, *2019*, CD012405.
6. Tsuboi, T.; Wong, J.K.; Eisinger, R.S.; Okromelidze, L.; Burns, M.R.; Ramirez-Zamora, A.; Almeida, L.; Shukla, A.W.; Foote, K.D.; Okun, M.S.; et al. Comparative connectivity correlates of dystonic and essential tremor deep brain stimulation. *Brain* **2021**, *144*, 1774–1786. [CrossRef]
7. Wu, H.; Hariz, M.; Visser-Vandewalle, V.; Zrinzo, L.; Coenen, V.A.; Sheth, S.A.; Bervoets, C.; Naesström, M.; Blomstedt, P.; Coyne, T.; et al. Deep brain stimulation for refractory obsessive-compulsive disorder (OCD): Emerging or established therapy? *Mol. Psychiatry* **2020**, *26*, 60–65. [CrossRef]
8. Le, H.T.; Haque, R.I.; Ouyang, Z.; Lee, S.W.; Fried, S.I.; Zhao, D.; Qiu, M.; Han, A. MEMS inductor fabrication and emerging applications in power electronics and neurotechnologies. *Microsyst. Nanoeng.* **2021**, *7*, 59. [CrossRef]
9. Lee, S.W.; Fried, S.I. Micro-magnetic stimulation of primary visual cortex induces focal and sustained activation of secondary visual cortex. *Philos. Trans. R. Soc. A* **2022**, *380*, 20210019. [CrossRef]
10. Lee, S.W.; Fallegger, F.; Casse, B.D.; Fried, S.I. Implantable microcoils for intracortical magnetic stimulation. *Sci. Adv.* **2016**, *2*, e1600889. [CrossRef]
11. Saha, R.; Faramarzi, S.; Bloom, R.P.; Benally, O.J.; Wu, K.; Di Girolamo, A.; Tonini, D.; Keirstead, S.A.; Low, W.C.; Netoff, T.I.; et al. Strength-frequency curve for micromagnetic neurostimulation through EPSPs on rat hippocampal neurons and numerical modeling of magnetic microcoil (μcoil). *J. Neural Eng.* **2022**, *19*, 016018. [CrossRef] [PubMed]
12. Bonmassar, G.; Lee, S.W.; Freeman, D.K.; Polasek, M.; Fried, S.I.; Gale, J.T. Microscopic magnetic stimulation of neural tissue. *Nat. Commun.* **2012**, *3*, 921. [CrossRef]
13. Osanai, H.; Minusa, S.; Tateno, T. Micro-coil-induced Inhomogeneous Electric Field Produces sound-driven-like Neural Responses in Microcircuits of the Mouse Auditory Cortex In Vivo. *Neuroscience* **2018**, *371*, 346–370. [CrossRef] [PubMed]
14. Minusa, S.; Muramatsu, S.; Osanai, H.; Tateno, T. A multichannel magnetic stimulation system using submillimeter-sized coils: System development and experimental application to rodent brain in vivo. *J. Neural Eng.* **2019**, *16*, 066014. [CrossRef] [PubMed]
15. Lee, S.W.; Fried, S.I. Enhanced Control of Cortical Pyramidal Neurons With Micromagnetic Stimulation. *IEEE Trans. Neural Syst. Rehabil. Eng.* **2017**, *25*, 1375–1386. [CrossRef]
16. Saha, R.; Sanger, Z.; Bloom, R.; Benally, O.J.; Wu, K.; Tonini, D.; Low, W.C.; Keirstead, S.A.; Netoff, T.I.; Wang, J.-P. Micromagnetic Stimulation (μMS) Dose-Response of the Rat Sciatic Nerve. *J. Neural Eng.* **2023**, *20*, 036022. [CrossRef]
17. Dong, L.; Li, G.; Tian, C.-X.; Lin, L.; Gao, Y.; Zheng, Y. Design of Submillimeter Magnetic Stimulation Instrumentation and Its Targeted Inhibitory Effect on Rat Model of Epilepsy. *IEEE Trans. Instrum. Meas.* **2021**, *70*, 4003708. [CrossRef]
18. FreeRTOS. Available online: https://www.freertos.org/ (accessed on 10 January 2023).
19. Minusa, S.; Osanai, H.; Tateno, T. Micromagnetic stimulation of the mouse auditory cortex in vivo using an implantable solenoid system. *IEEE Trans. Biomed. Eng.* **2018**, *65*, 1301–1310. [CrossRef]
20. Ye, H.; Chen, V.C.-F.; Helon, J.; Apostolopoulos, N. Focal Suppression of Epileptiform Activity in the Hippocampus by a High-frequency Magnetic Field. *Neuroscience* **2020**, *432*, 1–14. [CrossRef]
21. Golestanirad, L.; Gale, J.T.; Manzoor, N.F.; Park, H.J.; Glait, L.; Haer, F.; Kaltenbach, J.A.; Bonmassar, G. Solenoidal Micromagnetic Stimulation Enables Activation of Axons With Specific Orientation. *Front. Physiol.* **2018**, *9*, 724. [CrossRef]
22. Lee, S.W.; Fried, S.I. Magnetic control of cortical pyramidal neuron activity using a micro-coil. In Proceedings of the 2015 7th International IEEE/EMBS Conference on Neural Engineering (NER), Montpellier, France, 22–24 April 2015; pp. 268–271. [CrossRef]
23. Parnas, I.; Hochstein, S.; Parnas, H. Theoretical analysis of parameters leading to frequency modulation along an inhomogeneous axon. *J. Neurophysiol.* **1976**, *39*, 909–923. [CrossRef] [PubMed]
24. Wang, R.; Jin, C.; McEwan, A.; van Schaik, A. A programmable axonal propagation delay circuit for time-delay spiking neural networks. In Proceedings of the 2011 IEEE International Symposium of Circuits and Systems (ISCAS), Rio de Janeiro, Brazil, 15–18 May 2011; pp. 869–872.

25. Zierhofer, C.M. Analysis of a linear model for electrical stimulation of axons-critical remarks on the activating function concept. *IEEE Trans. Biomed. Eng.* **2001**, *48*, 173–184. [CrossRef] [PubMed]
26. Park, H.J.; Bonmassar, G.; Kaltenbach, J.A.; Machado, A.G.; Manzoor, N.F.; Gale, J.T. Activation of the central nervous system induced by micro-magnetic stimulation. *Nat. Commun.* **2013**, *4*, 2463. [CrossRef] [PubMed]